Modelling the steady-state of secondary control in islanded AC microgrids

Pompodakis, Evangelos E.; Tinajero, Gibran D.A.; Karapidakis, Emmanuel S.

Published in:
International Journal of Electrical Power and Energy Systems

DOI (link to publication from Publisher):
10.1016/j.ijepes.2023.109295

Publication date:
2023

Document Version
Publisher's PDF, also known as Version of record

Electrical Power and Energy Systems 153 (2023) 109295

Contents lists available at ScienceDirect

International Journal of Electrical Power and Energy Systems

journal homepage: www.elsevier.com/locate/ijepes

Modelling the steady-state of secondary control in islanded AC microgrids

Evangelos E. Pompodakis [a,*], Gibran D.A. Tinajero [b], Emmanuel S. Karapidakis [c]

[a] Post-doctoral Researcher in the Institute of Energy, Environment and Climatic Change, Hellenic Mediterranean University of Crete, Greece
[b] The Faculty of Engineering and Science Electric Power Systems and Microgrids, Aalborg University, Denmark
[c] School of Engineering, Hellenic Mediterranean University, Greece

ARTICLE INFO

Keywords:
Communication failures
Consensus algorithms
Cyberattacks
Frequency and voltage restoration
Hierarchical control
Islanded microgrids
Power flow
Secondary control

ABSTRACT

The secondary control is applied in islanded Microgrids (MGs), after the primary control, in order to restore the voltages and frequency to specified values. Although existing power flow methods can accurately calculate the power flow of primary and tertiary control of islanded MGs, they present considerable limitations in the modelling of secondary control. The main challenge is that secondary controllers consist of integral parts, which under communication failures, could integrate functions with different integral histories, and thus, can imply non-uniform power production of distributed generators (DGs). This paper proposes a power flow method for calculating, accurately, the steady-state of secondary control in islanded MGs. The method has four distinct features: a) generalized implementation in several communication strategies e.g., centralized, decentralized, consensus, distributed averaging, b) precise simulation of communication links and proportional-integral (PI) controllers, c) low computation time, and d) accurate three-phase network representation. Simulations were executed to validate the proposed method and highlight the importance of modelling, precisely, the secondary control in islanded MGs.

1. Introduction

Microgrids (MGs) are small scale networks consisting of controllable components that can operate in grid-connected or islanded mode. In islanded operation, the control objectives of a MG are performed by a hierarchical control scheme consisting of three layers: primary, secondary and tertiary [1].

1.1. Motivation and Challenges of Modelling the Secondary Control Layer

Accurate steady-state modelling of the three layers is crucial for the planning, design, operation, state estimation, supervision, contingency and stability analysis of islanded MGs. The modelling of the primary layer has been sufficiently investigated last years through three-phase [2–5] and single-phase power flow algorithms [6–13]. The tertiary layer usually outputs the optimal droop parameters (e.g., droop gains) to be applied in the primary layer [1], and therefore, primary power flow algorithms are sufficient for modelling the steady-state of tertiary layer, as well.

On the opposite, the secondary layer implements integral controllers (usually proportional-integral (PI) controllers) to eliminate the frequency and voltage deviations caused by the primary layer. The steady-state modelling of the secondary layer poses particular challenges, mainly, due to the following reasons: a) the integral parts of secondary controllers can (under certain circumstances like communication failures) affect the power production of DGs, due to the different integral histories, and b) the communication strategy (e.g., centralized, decentralized, consensus, distributed averaging) can significantly affect the steady state condition of an islanded MG. Unfortunately, the power flow algorithms of primary layer e.g. [2–13] are not adequate to model the action of secondary controllers, because they ignore both the integral parts and the communication strategy. Therefore, the development of new power flow algorithms, which will simulate, accurately, the steady state of secondary control is deemed necessary.

1.2. Literature Review and Contribution of the Paper

Last years, the research community has made efforts to develop accurate and efficient power flow approaches to calculate the steady-state of islanded MGs, considering their particular characteristics such as the absence of a slack bus, the droop curves of DGs, the variation of frequency etc. For instance, authors in [6–13] propose single-phase power

* Corresponding author.
E-mail address: bobodakis@hotmail.com (E.E. Pompodakis).

https://doi.org/10.1016/j.ijepes.2023.109295
Received 10 February 2023; Received in revised form 27 April 2023; Accepted 5 June 2023
Available online 22 June 2023

flow algorithms, while in [2–5], the power flow is solved, considering the network's unbalances.

Although the aforementioned methods can effectively simulate the steady-state of the primary and tertiary control, they cannot accurately model the secondary control, for the reasons referred in Section 1.1. Thus, the steady state modelling of secondary layer remains a totally unexplored topic. To the best of our knowledge, only three research works exist that consider the action of secondary controllers [18,26,27]. However, all of them present considerable limitations.

In [18], a single-phase Newton Raphson (NR)-based power flow approach was proposed that incorporates the action of secondary controllers. However, the method is only applicable in the centralized and not in decentralized, distributed averaging and consensus control. Moreover, it ignores possible communication failures between the DGs, the unbalance of the network, the pinning and operational modes of DGs, which can all lead to considerable inaccuracies under some circumstances. Finally, the inversion (or LU refactorization) of the Jacobian matrix increases significantly the computational time, when applied in large MGs (e.g $>$ 1000 Buses).

In [26–27], authors propose a backward forward sweep (BFS) and a NR power flow method, respectively. Nevertheless, they consider only the secondary voltage controllers and not the frequency controllers, which can significantly affect the accuracy of the simulation. Moreover, the pinning and communication between the DGs were completely neglected. Furthermore, both papers use single-phase formulation neglecting the MG unbalances. Finally, BFS method presents considerable limitations in highly (or weakly) meshed MGs, while NR has a long computation time in case of large Jacobian matrices.

To overcome the limitations of existing literature, this paper, presents a power flow approach with the following distinct features:

- It considers the accurate response of secondary frequency and voltage controllers. Thus, the steady state of the microgrid after the stabilization of secondary control is precisely computed.
- It considers, accurately, the communication links between the DGs, which enables, for first time, the calculation of power flow in case of communication failures between the DGs, cyberattacks, denial-of-services etc. Simulations in Sections 6 and 7 indicate that communication failures can significantly deteriorate the power sharing of DGs.
- It has generalized implementation in several control strategies e.g., centralized, decentralized, consensus, distributed averaging. Simulations indicate that the adopted control strategy can greatly affect the steady state of the MG and should be accurately considered.
- It presents low computation time, even in very large MGs.
- It considers, accurately, the 3-phase representation and the unbalance of the MG as well as the variety of operational modes of DGs e.g., balanced current, balanced voltages etc.

This paper is structured as follows: The hierarchical architecture is explained in Section 2. A generalized non-linear equation is proposed in Section 3, representing the most basic frequency and voltage control strategies. Section 4 quotes a simple example, while Section 5 proposes a generic method to compute the steady state of secondary controller. Simulation results are presented in Sections 6 and 7. Finally, Section 8 concludes the paper.

2. Hierarchical control of islanded microgrids

The three control layers of islanded MGs are shortly explained below:

2.1. Primary control

The primary layer has the fastest reaction and it is responsible to maintain frequency stability and balance between power generation and consumption. The primary control of DG i is mathematically expressed

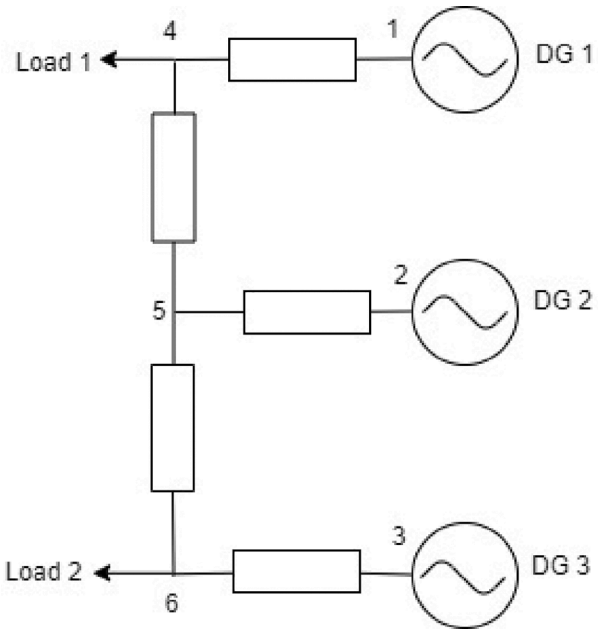

Fig. 1. 6-Bus islanded MG with two loads and 3 DGs.

by the following droop equations [2]:

$$\omega_i = \omega_{ref(i)} - K_{P(i)} \cdot P_{G(i)} + u_{p(i)} \quad (1)$$

$$V_i = V_{ref(i)} - K_{Q(i)} \cdot Q_{G(i)} + u_{q(i)} \quad (2)$$

where ω_i, $\omega_{ref(i)}$, $K_{P(i)}$, $P_{G(i)}$, V_i, $V_{ref(i)}$, $K_{Q(i)}$ and $Q_{G(i)}$ are the angular frequency measured by DG i, reference angular frequency of DG i, frequency droop gain, positive sequence active power output, positive sequence voltage magnitude, reference voltage, voltage droop gain, and positive sequence reactive power output of DG i, respectively. Additionally, $u_{p(i)}$ and $u_{q(i)}$ are the output signals of the secondary frequency and voltage controller, respectively.

Ideally, $u_{p(i)}$ should be equal for all DGs, so that their droop equations are equally displaced, ensuring a desired active power sharing between the DGs. However, under certain circumstances such as communication failures, the integral part of PI controllers of some DGs may imply different integral histories. As a consequence, $u_{p(i)}$ may differ in some DGs, deteriorating their power sharing.

2.2. Secondary Control

The objective of secondary layer is to eliminate the frequency and voltage deviations resulted from the primary layer. More specifically, the secondary controllers update the terms $u_{p(i)}$ and $u_{q(i)}$ in (1) and (2) in order to restore the frequency and voltage of DGs to the desired values. There are several control schemes for the secondary layer, the most important of which are explained in Section 3. The reaction time of secondary layer is slower than primary but faster than tertiary [28].

2.3. Tertiary Control

The tertiary control has the slowest reaction time (in the order of several minutes or even hours), and therefore, it does not require demanding communication infrastructure. It performs power and energy management, system optimization, economic dispatch etc. [28]. Practically, it calculates, periodically, the optimal parameters $K_{P(i)}, K_{Q(i)}, f_{ref(i)}, V_{ref(i)}$ of (1)–(2) in order to achieve an optimization objective, e.g., lowest generation cost.

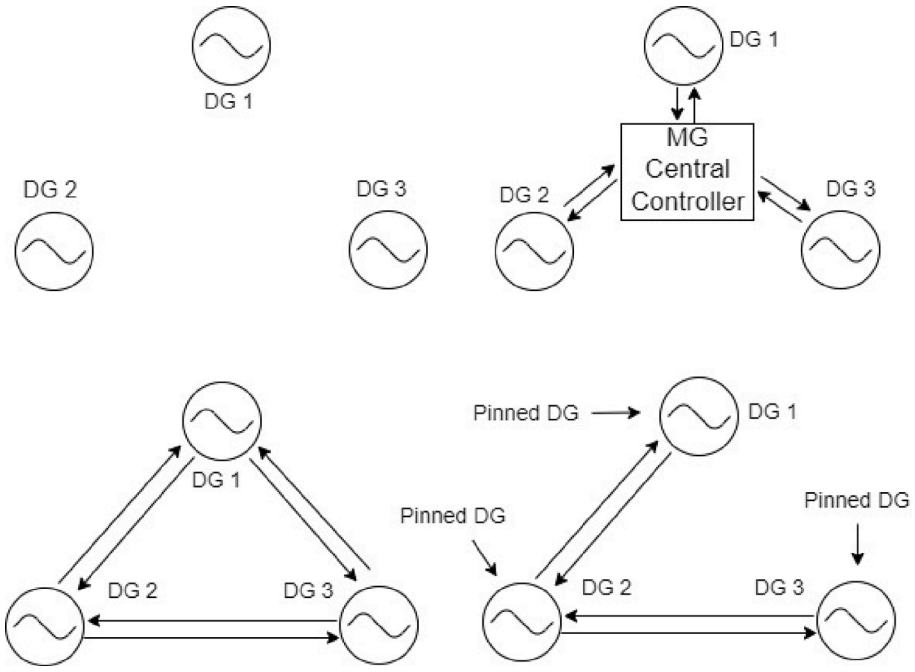

Fig. 2. Communication graphs of 6-Bus Microgrid. Top-left (a): Decentralized control, Top-right (b): Centralized control, Bottom-left (c): Distributed Averaging control, Bottom-right (d): Consensus control.

3. Generalized equation for secondary control

Secondary control strategies are categorized depending on their communication infrastructure and their control algorithms [14]. In Section 3.1, the basic control strategies of secondary layer are explained. All the basic strategies are mathematically summarized in one generalized equation in Section 3.2.

3.1. Formulation of the Basic Secondary Control Strategies

To facilitate the explanation, let us firstly assume the islanded MG of Fig. 1, consisting of three DGs.

3.1.1. Decentralized control

The decentralized communication scheme of the MG of Fig. 1 is depicted in Fig. 2a [15–17]. The DGs do not communicate with each other and their control is performed using only local measurements. Despite its simplicity, this control strategy is not recommended, because it performs uncontrollable power sharing between the DGs, as will be shown in Section 6. In decentralized control, the correction terms $u_{p(i)}$ and $u_{q(i)}$ of droop equations (1) and (2) are calculated from (3) and (4), $\forall$ $i \in \{1,2,3\}$ [17].

$$u_{p(i)} = K^{gain}_{p,pro(i)} \cdot (\omega_{set(i)} - \omega_i) + K^{gain}_{p,int(i)} \cdot \int (\omega_{set(i)} - \omega_i) \tag{3}$$

$$u_{q(i)} = K^{gain}_{q,pro(i)} \cdot (V_{set(i)} - V_i) + K^{gain}_{q,int(i)} \cdot \int (V_{set(i)} - V_i) \tag{4}$$

where $K^{gain}_{p,pro(i)}$ $K^{gain}_{p,int(i)}$, $K^{gain}_{q,pro(i)}$, $K^{gain}_{q,int(i)}$ are the proportional (pro) and integral (int) gains of the frequency (p) and voltage (q) controller of DG i. $\omega_{set(i)}$ and $V_{set(i)}$ are the desirable frequency and voltage that the controller attempts to reach. ω_i and V_i are the frequency and voltage measured, locally, from the controller of DG i.

3.1.2. Centralized Control

It is a kind of one-to-all communication structure, as shown in Fig. 2b [14,18]. A microgrid central controller (MGCC) measures the voltage and frequency in a specific point of the network (usually at the connection point of MGCC) and restores them using a single PI controller. The correction terms $u_{p(i)}$ and $u_{q(i)}$ in (1) and (2) are calculated from (5) and (6) $\forall$ $i \in \{1,2,3\}$ [14,18] [19, Fig. 3]:

$$u_{p(i)} = K^{gain}_{p,pro} \cdot (\omega_{set} - \omega_{MGCC}) + K^{gain}_{p,int} \cdot \int (\omega_{set} - \omega_{MGCC}) \tag{5}$$

$$u_{q(i)} = K^{gain}_{q,pro} \cdot (V_{set} - V_{MGCC}) + K^{gain}_{q,int} \cdot \int (V_{set} - V_{MGCC}) \tag{6}$$

where $K^{gain}_{p,pro}$ $K^{gain}_{p,int}$, $K^{gain}_{q,pro}$, $K^{gain}_{q,int}$ are the proportional and integral gains of MGCC. ω_{MGCC} and V_{MGCC} are the angular frequency and voltage measured by the MGCC. ω_{set} and V_{set} are the desirable frequency and voltage values of MGCC. It is shown from (5)–(6) that all DGs receive the same $u_{p(i)}$, $u_{q(i)}$ values from the MGCC, and thus, they shift, equally, their droop equations preserving a desired power sharing, depending on their size and cost.

As an example, Fig. 3 depicts the action of centralized secondary controller on the droop curves of DGs. Before the load rise, the system has been stabilized at the nominal frequency (50 Hz), as shown in Fig. 3a. The power is shared from the DGs according to their droop gains, which are usually computed by the tertiary control, considering the size and fuel cost of DGs. In this example, $K_{P(1)} < K_{P(2)} < K_{P(3)}$, and thus, DG 1 undertakes a higher load. After a load rise (ΔP_L), primary control instantaneously acts to force DGs undertake equally the extra load, while the frequency deviates from the nominal value (46 Hz), as shown in Fig. 3b. After some seconds, secondary control is activated, by shifting equally the three curves by $u_{p(i)}$ $\forall$ DG i, as shown in Fig. 3c. In this way, the frequency is restored, while the desired power sharing between the DGs is preserved, namely $\frac{P'_{G(1)}}{P_{G(1)}} = \frac{P'_{G(2)}}{P_{G(2)}} = \frac{P'_{G(3)}}{P_{G(3)}}$. However, in case that the communication link between MGCC and DG 1 is out of service (e.g., due to a damage or cyberattack etc.), the command $u_{p(1)}$ is not sent to DG 1 (namely $u_{p(1)} = 0$), and thus, the load rise is covered only by DG 2 and DG 3, as shown in Fig. 3c. In that case, the load sharing of DGs is completely lost since $P''_{G(2)} > P''_{G(1)}$.

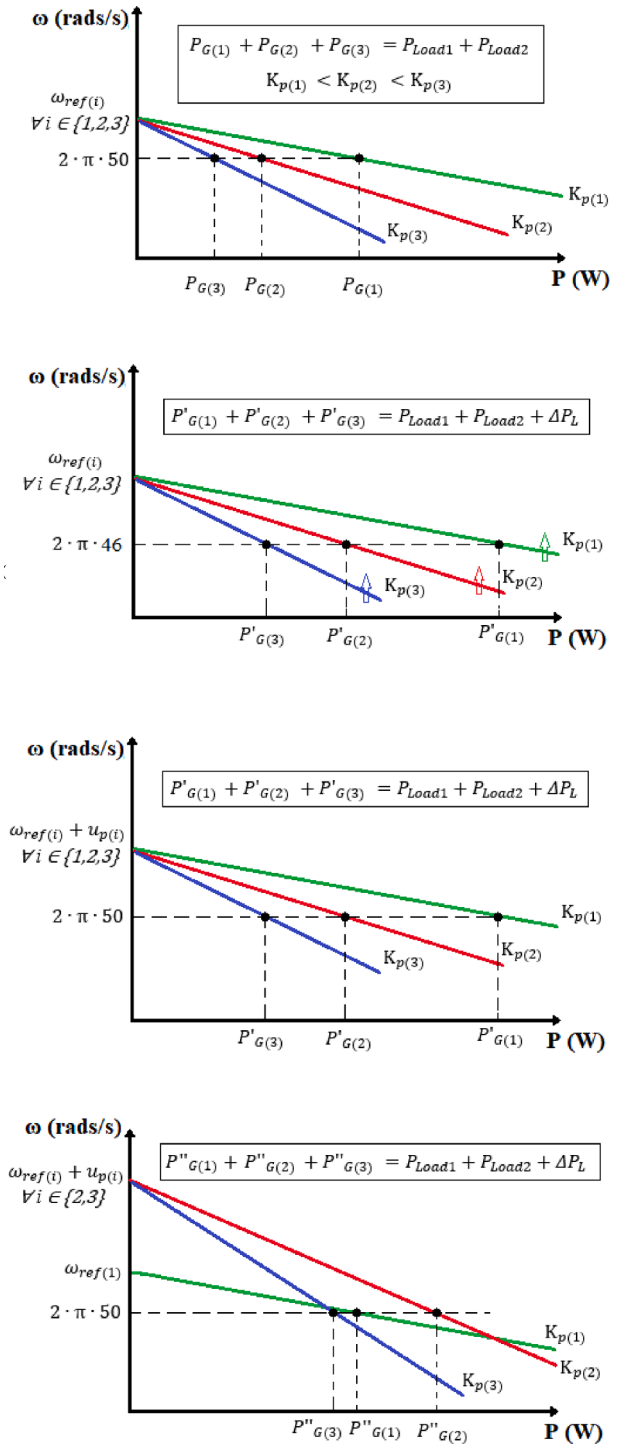

Fig. 3. Centralized secondary control of 6-Bus network: From top to bottom: a) before the load rise, b) after the load rise and before the activation of secondary control, b) after the activation of secondary control without communication failures, c) after the activation of secondary control with an outage of link between DG 1 and MGCC.

3.1.3. Distributed Averaging Control

It is a kind of all-to-all communication structure, as shown in Fig. 2c [19,20]. Each DG measures its local frequency, voltage and reactive power and send (receives) them to (from) all the other DGs. The DGs average the received signals and restore them using their own local PI controllers. The mathematical equations of $u_{p(i)}$ and $u_{q(i)}$ of each DG are expressed by (7) and (8) $\forall\, i \in \{1,2,3\}$ [19 20].

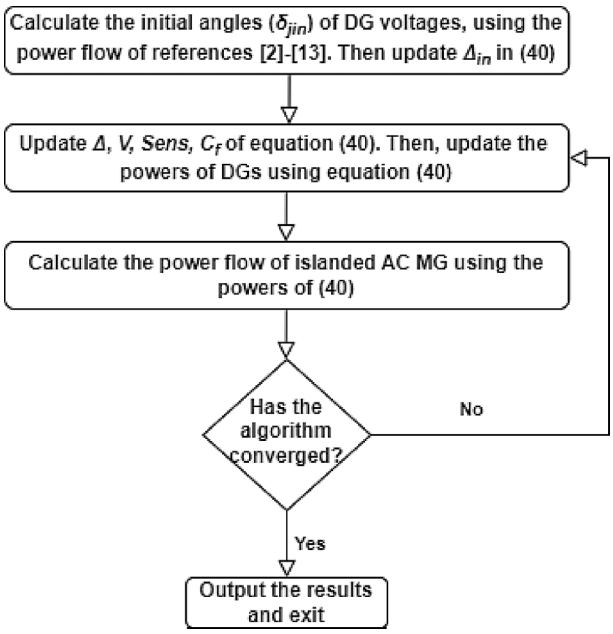

Fig. 4. Flowchart of the proposed approach.

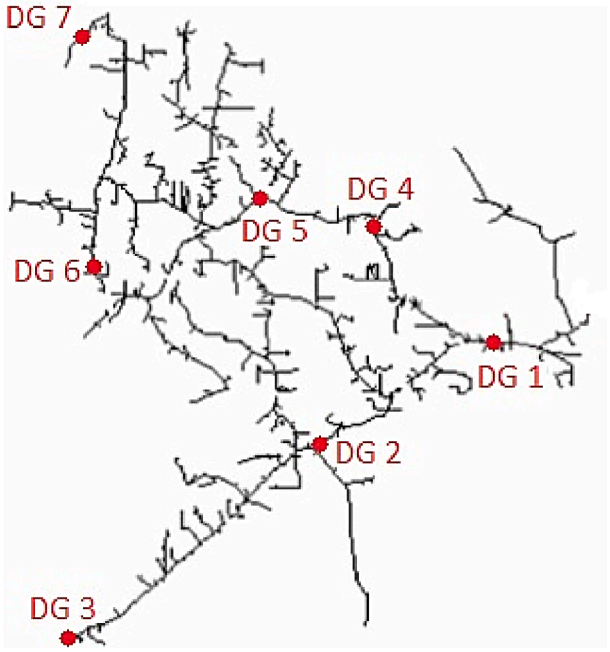

Fig. 5. Islanded IEEE 8500-Node network with 7 DGs.

$$u_{p(i)} = K^{gain}_{p,pro(i)} \cdot (\omega_{set} - \bar{\omega}_i) + K^{gain}_{p,int(i)} \cdot \int (\omega_{set} - \bar{\omega}_i) \tag{7}$$

$$u_{q(i)} = K^{gain}_{v,pro(i)} \cdot (V_{set} - \bar{V}_i) + K^{gain}_{v,int(i)} \cdot \int (V_{set} - \bar{V}_i) K^{gain}_{q,pro(i)} \cdot (\bar{Q}_i - Q_{G(i)}) + K^{gain}_{q,int(i)} \cdot \int (\bar{Q}_i - Q_{G(i)}) \tag{8}$$

where $\bar{\omega}_i, \bar{V}_i, \bar{Q}_i$ are the averaged values of frequency, voltage and reactive power, respectively, received by all DGs and are expressed as follows: $\bar{\omega}_i = \frac{\sum_{i=1}^{N_{dg}} \omega_i}{N_{dg}}$, $\bar{V}_i = \frac{\sum_{i=1}^{N_{dg}} V_i}{N_{dg}}$, $\bar{Q}_i = \frac{\sum_{i=1}^{N_{dg}} Q_{G(i)}}{N_{dg}}$, where N_{dg} is the total number of DGs. ω_i, $V_i, Q_{G(i)}$ are respectively the angular frequency,

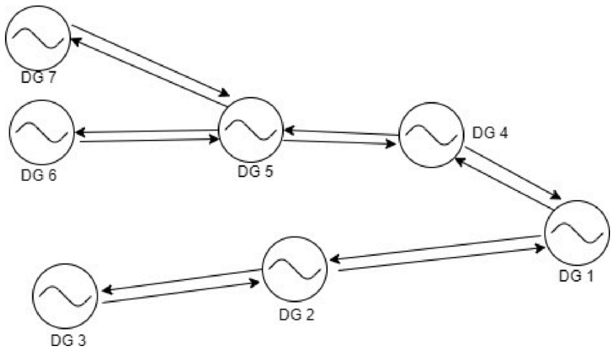

Fig. 6. Communication graph of islanded IEEE 8500-Node network.

voltage and reactive power of DG i. More details are provided in [19, Fig. 5].

3.1.4. Consensus Control

In the consensus control, DGs communicate only with some neighboring DGs and not with all DGs, as is the case of distributed averaging [21–25]. It is a type of neighbor-to-neighbor communication with a structure shown in Fig. 2d.

The consensus equations can be linear [21–25,33] or non-linear [29]. Nevertheless, in this paper, only the linear consensus is considered, while the non-linear is left for future research. In consensus algorithms, the frequency controller performs, simultaneously, frequency restoration and active power sharing between the DGs [22, Fig. 6], while voltage controller executes voltage restoration or reactive power sharing.

Two of the most basic linear consensus control schemes are the models of Bidram et. Al [22] and Simpson et. Al [24]. Although other linear equations have been presented in the literature, e.g., [21,23,25,32–36], they are variations of these two basic models. Below, the consensus frequency and voltage controllers of Bidram [22] and Simpson [24] are presented, in two different sub-sections.

3.1.4.1. Consensus controller of Bidram [22]. The block diagram of Bidram's frequency controller is depicted in [22, Fig. 6]. It performs, simultaneously, frequency regulation and equal active power sharing and it is mathematically expressed by (9) $\forall\, i \in \{1,2,3\}$.

$$u_{p(i)} = K^{gain}_{p,int(i)} \cdot \int \Bigg(g_i \cdot (\omega_{set} - \omega_i) + \sum_{j=1}^{N_{dg}} a_{ij} \cdot (\omega_j - \omega_i) + \sum_{j=1}^{N_{dg}} d_{ij} \cdot \big(-\omega_{ref(j)} + K_{P(j)} \cdot P_{G(j)} + \omega_{ref(i)} - K_{P(i)} \cdot P_{G(i)} \big) \Bigg) \tag{9}$$

The value of g_i indicates the access of DG i to the desirable frequency (ω_{set}). If $g_i = 0$, DG i does not have access to this information. The value of a_{ij} and d_{ij} depends on the connectivity between DG i and j. More specifically, if DG i communicates directly (through a wired or wireless link) with DG j, then $d_{ij}, a_{ij} \neq 0$, otherwise they are both zeros [22]. $K_{P(i)}$, $K_{Q(i)}$, $P_{G(i)}$, $Q_{G(i)}$ are the primary droop gains and powers of DGs (see eq. (1) and (2)).

The Bidram's voltage controller regulates the voltage at the desired value ($V_{set(i)}$). The mathematical expression is shown in (10) $\forall\, i \in \{1,2,3\}$. If DG i has access to the reference value $h_i \neq 0$, otherwise it is zero. If DG i communicates directly with DG j, then $c_{ij} \neq 0$, otherwise it is zero. $K^{gain}_{p,int(i)}$ and $K^{gain}_{q,int(i)}$ are the integral gains of the frequency and voltage controller, respectively.

$$u_{q(i)} = K^{gain}_{q,int(i)} \cdot \int \Bigg(h_i \cdot (V_{set(i)} - V_i) + \sum_{j=1}^{N_{dg}} c_{ij} \cdot (V_j - V_i) \Bigg) \tag{10}$$

3.1.4.2. Consensus controller of Simpson [24]. The mathematical expression of Simpson's frequency controller is quoted in (11) $\forall\, i \in \{1,2,3\}$. g_i determines the access of DG i to the desired frequency (ω_{set}). β_{ij} depends on the connectivity between DG i and j. If DG i communicates directly with DG j, then $\beta_{ij} \neq 0$, otherwise it is zero.

$$u_{p(i)} = K^{gain}_{p,int(i)} \cdot \int \Bigg(g_i \cdot (\omega_{set} - \omega_i) + \sum_{j=1}^{N_{dg}} \beta_{ij} \cdot (u_{p(j)} - u_{p(i)}) \Bigg) \tag{11}$$

The Simpson's voltage controller is expressed by (12) $\forall\, i \in \{1,2,3\}$. Simpson examines 2 cases for the voltage controller, by varying the h_i and r_{ij} values, depending on weather the controller performs voltage regulation ($h_i \neq 0$, $r_{ij} = 0$) or optimal reactive power sharing ($h_i = 0$, $r_{ij} \neq 0$). For more details, please refer to [24, Section 4.3].

$$u_{q(i)} = K^{gain}_{q,int(i)} \cdot \int \Bigg(h_i \cdot (V_{set(i)} - V_i) + \sum_{j=1}^{N_{dg}} r_{ij} \cdot \big(K_{Q(j)} \cdot Q_{G(j)} - K_{Q(i)} \cdot Q_{G(i)} \big) \Bigg) \tag{12}$$

Table 1
Vectors and Matrices of the Generalized Equation (16) of Frequency Controller for all Control Strategies.

Decentralized	Centralized	Distributed Averaging	Consensus Bidram [22]	Consensus Simpson [24]
$\mathbf{g}=[1\ \ 1\ \ 1]$	$\mathbf{g}=[1\ \ 1\ \ 1]$	$\mathbf{g}=[1\ \ 1\ \ 1]$	$\mathbf{g}=[1\ \ 1\ \ 1]$ *	$\mathbf{g}=[1\ \ 1\ \ 1]$ *
$\boldsymbol{\alpha} = \begin{bmatrix} 0 & 0 & 0 \\ 0 & 0 & 0 \\ 0 & 0 & 0 \end{bmatrix}$	$\boldsymbol{\alpha} = \begin{bmatrix} 0 & 0 & 0 \\ -1 & -1 & 0 \\ -1 & 0 & -1 \end{bmatrix}$	$\boldsymbol{\alpha} = -\begin{bmatrix} 2/3 & 1/3 & 1/3 \\ 1/3 & 2/3 & 1/3 \\ 1/3 & 1/3 & 2/3 \end{bmatrix}$	$\boldsymbol{\alpha} = \begin{bmatrix} 1 & 1 & 0 \\ 1 & 2 & 1 \\ 0 & 1 & 1 \end{bmatrix}$	$\boldsymbol{\alpha} = \begin{bmatrix} 0 & 0 & 0 \\ 0 & 0 & 0 \\ 0 & 0 & 0 \end{bmatrix}$
$\boldsymbol{\beta} = \begin{bmatrix} 0 & 0 & 0 \\ 0 & 0 & 0 \\ 0 & 0 & 0 \end{bmatrix}$	$\boldsymbol{\beta} = \begin{bmatrix} 0 & 0 & 0 \\ 0 & 0 & 0 \\ 0 & 0 & 0 \end{bmatrix}$	$\boldsymbol{\beta} = \begin{bmatrix} 0 & 0 & 0 \\ 0 & 0 & 0 \\ 0 & 0 & 0 \end{bmatrix}$	$\boldsymbol{\beta} = \begin{bmatrix} 0 & 0 & 0 \\ 0 & 0 & 0 \\ 0 & 0 & 0 \end{bmatrix}$	$\boldsymbol{\beta} = \begin{bmatrix} 1 & 1 & 0 \\ 1 & 2 & 1 \\ 0 & 1 & 1 \end{bmatrix}$
$\mathbf{d} = \begin{bmatrix} 0 & 0 & 0 \\ 0 & 0 & 0 \\ 0 & 0 & 0 \end{bmatrix}$	$\mathbf{d} = \begin{bmatrix} 0 & 0 & 0 \\ 0 & 0 & 0 \\ 0 & 0 & 0 \end{bmatrix}$	$\mathbf{d} = \begin{bmatrix} 0 & 0 & 0 \\ 0 & 0 & 0 \\ 0 & 0 & 0 \end{bmatrix}$	$\mathbf{d} = \begin{bmatrix} 1 & 1 & 0 \\ 1 & 2 & 1 \\ 0 & 1 & 1 \end{bmatrix}$	$\mathbf{d} = \begin{bmatrix} 0 & 0 & 0 \\ 0 & 0 & 0 \\ 0 & 0 & 0 \end{bmatrix}$

*All DGs are assumed pinned namely they have access to reference values. In case that a DG is unpinned, the corresponding element is zero.

Table 2
Vectors and Matrices of the Generalized Equation (14) of Voltage Controller for all Control Strategies.

Decentralized	Centralized	Distributed Averaging	Consensus - Bidram [22]	Consensus - Simpson [24] **	
				Case 1 (reactive power sharing)	Case 2 (voltage regulation)
$\mathbf{h}=[1\ \ 1\ \ 1]$ $\boldsymbol{c}=\begin{bmatrix}0&0&0\\0&0&0\\0&0&0\end{bmatrix}$ $\boldsymbol{r}=\begin{bmatrix}0&0&0\\0&0&0\\0&0&0\end{bmatrix}$	$\mathbf{h}=[1\ \ 1\ \ 1]$ $\boldsymbol{c}=\begin{bmatrix}0&0&0\\-1&-1&0\\-1&0&-1\end{bmatrix}$ $\boldsymbol{r}=\begin{bmatrix}0&0&0\\0&0&0\\0&0&0\end{bmatrix}$	$\mathbf{h}=[1\ \ 1\ \ 1]$ $\boldsymbol{c}=-\begin{bmatrix}2/3&1/3&1/3\\1/3&2/3&1/3\\1/3&1/3&2/3\end{bmatrix}$ $\boldsymbol{r}=\begin{bmatrix}2/3&1/3&1/3\\1/3&2/3&1/3\\1/3&1/3&2/3\end{bmatrix}$	$\mathbf{h}=[1\ \ 1\ \ 1]$ * $\boldsymbol{c}=\begin{bmatrix}1&1&0\\1&2&1\\0&1&1\end{bmatrix}$ $\boldsymbol{r}=\begin{bmatrix}0&0&0\\0&0&0\\0&0&0\end{bmatrix}$	$\mathbf{h}=[0\ \ 0\ \ 0]$ $\boldsymbol{c}=\begin{bmatrix}0&0&0\\0&0&0\\0&0&0\end{bmatrix}$ $\boldsymbol{r}=\begin{bmatrix}1&1&0\\1&2&1\\0&1&1\end{bmatrix}$	$\mathbf{h}=[1\ \ 1\ \ 1]$ * $\boldsymbol{c}=\begin{bmatrix}0&0&0\\0&0&0\\0&0&0\end{bmatrix}$ $\boldsymbol{r}=\begin{bmatrix}0&0&0\\0&0&0\\0&0&0\end{bmatrix}$

*All DGs are assumed pinned namely they have access to reference values. In case that a DG is unpinned, the corresponding element is zero.
**Simpson proposes 2 different cases, with different objectives, for the secondary voltage controller (refer [24, Section 4.3]).

3.2. Proposed generalized formulation representing all secondary control strategies

Equations (3), (5), (7), (9) and (11) can be written in a compact and generalized form, as shown in (13). Similarly, equations (4), (6), (8), (10), (12) can be expressed through the generalized form of (14). The values of $g_i, a_{ij}, \beta_{ij}, d_{ij}, h_i, c_{ij}, r_{ij}$ are selected depending on the control mode e.g decentralized, centralized, distributed averaging, consensus etc. Note that the proportional part of controllers is not expressed in (13)–(14) since, after the restoration, the proportional term of PI controller is nullified.

For example, let us assume the network of Fig. 1, which can be controlled in one of the modes of Fig. 2. Depending on the control mode, the secondary frequency and voltage controller can be mathematically expressed from (13) and (14), respectively, using the $g_i, a_{ij}, \beta_{ij}, d_{ij}, h_i, c_{ij}, r_{ij}$ of Tables 1 and 2. It is clarified that a_{ij} is the element that is located in the ith row and jth column of $\boldsymbol{\alpha}$ matrix of Table 1. Similarly, for the other matrices.

The right-hand side of (13) contains the terms $u_{p(i)}, u_{q(i)}$, which are replaced by $u_{p(i)} = \omega_i - \omega_{ref(i)} + K_{P(i)} \cdot P_{G(i)}$ (based on (1)–(2)), deriving equation (15). After a simple reformation, equation (15) is simplified to (16), which is the generalized equation of secondary frequency controller, including all the basic control schemes, e.g., decentralized, consensus etc.

$$u_{p(i)} = K_{p,int(i)}^{gain} \cdot \int \left(g_i \cdot (\omega_{set} - \omega_i) + \sum_{j=1}^{N_{dg}} a_{ij} \cdot (\omega_j - \omega_i) + \sum_{j=1}^{N_{dg}} \beta_{ij} \cdot (u_{p(j)} - u_{p(i)}) + \sum_{j=1}^{N_{dg}} d_{ij} \cdot (-\omega_{ref(j)} + K_{P(j)} \cdot P_{G(j)} + \omega_{ref(i)} - K_{P(i)} \cdot P_{G(i)}) \right) \tag{13}$$

Table 3
Steady State Results of Primary Control of 6-Bus MG.

	Reference [3]	Simulink
Frequency (Hz)	49.8974	49.8974
Voltage DG 1 (V)	227.5605	227.5605
Voltage DG 2 (V)	227.9016	227.9016
Voltage DG 3 (V)	224.7220	224.7220
Voltage angle DG 1 (rads) (δ_{1in})	0.7854	–*
Voltage angle DG 2 (rads) (δ_{2in})	0.7846	–*
Voltage angle DG 3 (rads) (δ_{3in})	0.7760	–*
Active/Reactive power DG 1 (kW/kVar)	51.3 / 12.2	51.3 / 12.2
Active/Reactive power DG 2 (kW/kVar)	51.3 / 10.5	51.3 / 10.5
Active/Reactive power DG 3 (kW/kVar)	51.3 / 26.4	51.3 / 26.4

*Simulink is a time-domain tool and does not compute voltage angles.

$$u_{q(i)} = K_{q,int(i)}^{gain} \cdot \int \left(h_i \cdot (V_{set(i)} - V_i) + \sum_{j=1}^{N_{dg}} c_{ij} \cdot (V_j - V_i) + \sum_{j=1}^{N_{dg}} r_{ij} \cdot (K_{Q(j)} \cdot Q_{G(j)} - K_{Q(i)} \cdot Q_{G(i)}) \right) \tag{14}$$

$$u_{p(i)} = K_{p,int(i)}^{gain} \cdot \int \left(g_i \cdot (\omega_{set} - \omega_i) + \sum_{j=1}^{N_{dg}} a_{ij} \cdot (\omega_j - \omega_i) + \sum_{j=1}^{N_{dg}} \beta_{ij} \cdot (\omega_j - \omega_{ref(j)} + K_{P(j)} \cdot P_{G(j)} - \omega_i + \omega_{ref(i)} - K_{P(i)} \cdot P_{G(i)}) + \sum_{j=1}^{N_{dg}} d_{ij} \cdot (-\omega_{ref(j)} + K_{P(j)} \cdot P_{G(j)} + \omega_{ref(i)} - K_{P(i)} \cdot P_{G(i)}) \right) \tag{15}$$

$$u_{p(i)} = K_{p,int(i)}^{gain} \cdot \int \left(g_i \cdot (\omega_{set} - \omega_i) + \sum_{j=1}^{N_{dg}} (a_{ij} + \beta_{ij}) \cdot (\omega_j - \omega_i) \right) + K_{p,int(i)}^{gain} \cdot \int \left(\sum_{j=1}^{N_{dg}} (\beta_{ij} + d_{ij}) \cdot (-\omega_{ref(j)} + K_{P(j)} \cdot P_{G(j)} + \omega_{ref(i)} - K_{P(i)} \cdot P_{G(i)}) \right) \tag{16}$$

4. A Simple Example in the 6-Bus Network

Here, a simple example is quoted to explain how the steady state of secondary control is computed, using the 6-Bus network of Fig. 1 with the parameters of Table 5. Only decentralized control is assumed here, while the generic method, with generalized implementation in all control strategies, is quoted in the next section.

As a first step, the power flow of the primary control is computed using a conventional algorithm, e.g., [2–13]. The results are depicted in Table 3. As shown, in primary control, the voltage and frequency of DGs deviate from the desired 50 Hz and 230 V values.

When decentralized secondary control is activated, equations (1)–(4) are combined to derive (17)–(18) $\forall\, i \in \{1,2,3\}$. After the stabilization of secondary controller, the frequency and voltage have been restored to their desired values, according to (19)–(20).

$$\omega_i = \omega_{ref(i)} - K_{P(i)} \cdot P_{G(i)} + K_{p,pro(i)}^{gain} \cdot (\omega_{set(i)} - \omega_i) + K_{p,int(i)}^{gain} \cdot \int (\omega_{set(i)} - \omega_i) \qquad \forall\, i \in \{1,2,3\} \tag{17}$$

$$V_i = V_{ref(i)} - K_{Q(i)}\cdot Q_{G(i)} + K^{gain}_{q,pro(i)}\cdot(V_{set(i)} - V_i) + K^{gain}_{q,int(i)}\cdot\int(V_{set(i)} - V_i) \qquad \forall i \in \{1,2,3\} \tag{18}$$

$$\omega_i = \omega_{ref(i)} = \omega_{set(i)} = 2\pi\cdot 50\ rads/s \qquad \forall i \in \{1,2,3\} \tag{19}$$

$$V_i = V_{ref(i)} = V_{set(i)} \qquad \forall i \in \{1,2,3\} \tag{20}$$

Combining (17)–(20), equations (21)–(22) are derived. Furthermore, the non-linear power flow equations of the 6-bus network are expressed in a compact form in (23). Equation system (21)–(23) expresses, mathematically, the steady state of decentralized secondary control. To the best of our knowledge, existing algorithms are not able to solve this system due to two difficulties: First, non-linear solvers, e.g., implicit Z_{BUS} [2,3], Newton-Trust-Region [4], NR [5] etc., do not solve integrals. Second, ω_i in (21) is not a power flow variable, making the system underdetermined (less equations than variables).

$$K_{P(i)}\cdot P_{G(i)} = K^{gain}_{p,int(i)}\cdot\int(\omega_{set(i)} - \omega_i) \qquad \forall i \in \{1,2,3\} \tag{21}$$

$$K_{Q(i)}\cdot Q_{G(i)} = K^{gain}_{q,int(i)}\cdot\int(V_{set(i)} - V_i) \qquad \forall i \in \{1,2,3\} \tag{22}$$

$$f(\boldsymbol{V}_1,...,\boldsymbol{V}_6,\boldsymbol{\delta}_1,...,\boldsymbol{\delta}_6,...,\boldsymbol{P}_1,...,\boldsymbol{P}_6,\boldsymbol{Q}_1,...,\boldsymbol{Q}_6) = 0 \tag{23}$$

To overcome these difficulties, (22) is linearized in (24), replacing the integral with the term ∞ that practically denotes an infinite number, e.g., 10^{10}. Physically, (24) forces $Q_{G(i)}$ to get a proper value so that $V_{set(i)} = V_i$.

$$K_{Q(i)}\cdot Q_{G(i)} = K^{gain}_{q,int(i)}\cdot\infty\cdot(V_{set(i)} - V_i) \qquad \forall i \in \{1,2,3\} \tag{24}$$

The integral of (21) is linearized using the equation proposed in [18, section 3.1]: $\int\left(\omega_{set(j)} - \omega_j\right) = \delta_{jin} - \delta_j\ \forall\ j = \{1,2,3\}$, where δ_{jin} is the initial (*in*) voltage angle of DG *j*, before the action of secondary control. This value is given in Table 3. δ_j is the voltage angle after the stabilization of secondary control. A physical explanation of $\int(\omega_{set} - \omega_j) = \delta_{jin} - \delta_j$ is given in Appendix A. With this equation, two objectives are achieved: First, the integral is eliminated, and second, ω_i is converted to a power flow variable (δ_j), making the system (21)–(23) solvable.

Applying the aforementioned linearizations, equation system (21)–(23) is modified to (25)–(27), which can be easily solved using conventional non-linear solvers. The results are shown in Table 4, assuming $K^{gain}_{p,int(i)} = K^{gain}_{q,int(i)} = 4$.

$$K_{P(j)}\cdot P_{G(j)} = K^{gain}_{p,int(j)}\cdot(\delta_{jin} - \delta_1) \qquad \forall j \in \{1,2,3\} \tag{25}$$

$$K_{Q(i)}\cdot Q_{G(i)} = K^{gain}_{q,int(i)}\cdot\infty\cdot(V_{set(i)} - V_i) \qquad \forall i \in \{1,2,3\} \tag{26}$$

$$f(\boldsymbol{V}_1,...,\boldsymbol{V}_6,\boldsymbol{\delta}_1,...,\boldsymbol{\delta}_6,...,\boldsymbol{P}_1,...,\boldsymbol{P}_6,\boldsymbol{Q}_1,...,\boldsymbol{Q}_6) = 0 \tag{27}$$

5. Proposed Generalized Steady-State Calculation of Secondary Control

The proposed approach is described in this section, which has a general implementation in all control strategies regardless the number of buses and DGs. Specifically, in Section 5.1, a short overview of the applied primary power flow algorithm is given. The proposed modelling approach of secondary control is described in Section 5.2, while Section 5.3 quotes a flowchart.

5.1. Power Flow algorithm

A power flow algorithm is needed to compute the steady state of primary control and angles $\delta_{jin}\ \forall j \in N_{dg}$ (N_{dg} is the number of DGs), as explained in Section 4. The algorithm of [3] is applied here, although other algorithms can be used as well, e.g., [2,4–13]. Nevertheless, the methods of [2–13] are only applicable for simulating the primary (and tertiary) control of islanded MGs, and not the secondary. The reason is that they compute the DG powers, from the droop equations (1)–(2), assuming that $u_{p(i)} = u_{p(i)} = 0$, ignoring the action of secondary control. In the next subsection, a generalized formulation is proposed to update the powers of DGs, considering the action of secondary controllers.

5.2. DG Powers of Secondary Control

The equation that calculates the positive-sequence active power of DGs is quoted in sub-section 5.2.1 and the reactive power in 5.2.2. Both equations are written in a unified mathematical form in sub-section 5.2.3. For the sake of clarity, the analysis below concerns the MG of Fig. 1, but it can be easily extended to larger MGs as well.

5.2.1. Calculation of DG active power

Substituting the generalized equation (16) into the droop equation (1), equation system (28) is obtained for the secondary frequency control of the examined 6-bus MG. In (28), $a_{ij}, \beta_{ij}, d_{ij}, g_i$, are given in Table 1, depending on the applied control strategy e.g decentralized, centralized, etc.

$$\begin{bmatrix}\omega_{ref(1)}-\omega_1\\ \omega_{ref(2)}-\omega_2\\ \omega_{ref(3)}-\omega_3\end{bmatrix} - \begin{bmatrix}K_{P(1)} & 0 & 0\\ 0 & K_{P(2)} & 0\\ 0 & 0 & K_{P(3)}\end{bmatrix}\cdot\begin{bmatrix}P_{G(1)}\\ P_{G(2)}\\ P_{G(3)}\end{bmatrix} = \begin{bmatrix}(a_{11}+\beta_{11}+g_1)\cdot K^{gain}_{p,int(1)} & -(a_{12}+\beta_{12})\cdot K^{gain}_{p,int(1)} & -(a_{13}+\beta_{13})\cdot K^{gain}_{p,int(1)}\\ -(a_{21}+\beta_{21})\cdot K^{gain}_{p,int(2)} & (a_{22}+\beta_{22}+g_2)\cdot K^{gain}_{p,int(2)} & -(a_{23}+\beta_{23})\cdot K^{gain}_{p,int(2)}\\ -(a_{31}+\beta_{31})\cdot K^{gain}_{p,int(3)} & -(a_{32}+\beta_{32})\cdot K^{gain}_{p,int(3)} & (a_{33}+\beta_{33}+g_3)\cdot K^{gain}_{p,int(3)}\end{bmatrix}\cdot\begin{bmatrix}\int(\omega_1-\omega_{set})\\ \int(\omega_2-\omega_{set})\\ \int(\omega_3-\omega_{set})\end{bmatrix}$$
$$-\begin{bmatrix}(\beta_{11}+d_{11})\cdot K^{gain}_{p,int(1)} & -(\beta_{12}+d_{12})\cdot K^{gain}_{p,int(1)} & -(\beta_{13}+d_{13})\cdot K^{gain}_{p,int(1)}\\ -(\beta_{21}+d_{21})\cdot K^{gain}_{p,int(2)} & (\beta_{22}+d_{22})\cdot K^{gain}_{p,int(2)} & -(\beta_{23}+d_{23})\cdot K^{gain}_{p,int(2)}\\ -(\beta_{31}+d_{31})\cdot K^{gain}_{p,int(3)} & -(\beta_{32}+d_{32})\cdot K^{gain}_{p,int(3)} & (\beta_{33}+d_{33})\cdot K^{gain}_{p,int(3)}\end{bmatrix}\cdot\begin{bmatrix}\int(\omega_{ref(1)}-K_{P(1)}\cdot P_{G(1)})\\ \int(\omega_{ref(2)}-K_{P(2)}\cdot P_{G(2)})\\ \int(\omega_{ref(3)}-K_{P(3)}\cdot P_{G(3)})\end{bmatrix} \tag{28}$$

$$\begin{bmatrix} \omega_{ref(1)}-\omega_{st} \\ \omega_{ref(2)}-\omega_{st} \\ \omega_{ref(3)}-\omega_{st} \end{bmatrix} - \begin{bmatrix} K_{P(1)} & 0 & 0 \\ 0 & K_{P(2)} & 0 \\ 0 & 0 & K_{P(3)} \end{bmatrix} \cdot \begin{bmatrix} P_{G(1)} \\ P_{G(2)} \\ P_{G(3)} \end{bmatrix} = \begin{bmatrix} (a_{11}+\beta_{11}+g_1)\cdot K^{gain}_{p,int(1)} & -(a_{12}+\beta_{12})\cdot K^{gain}_{p,int(1)} & -(a_{13}+\beta_{13})\cdot K^{gain}_{p,int(1)} \\ -(a_{21}+\beta_{21})\cdot K^{gain}_{p,int(2)} & (a_{22}+\beta_{22}+g_2)\cdot K^{gain}_{p,int(2)} & -(a_{23}+\beta_{23})\cdot K^{gain}_{p,int(2)} \\ -(a_{31}+\beta_{31})\cdot K^{gain}_{p,int(3)} & -(a_{32}+\beta_{32})\cdot K^{gain}_{p,int(3)} & (a_{33}+\beta_{33}+g_3)\cdot K^{gain}_{p,int(3)} \end{bmatrix} \cdot \begin{bmatrix} \delta_1-\delta_{1in} \\ \delta_2-\delta_{2in} \\ \delta_3-\delta_{3in} \end{bmatrix} - 10^{10}\cdot$$
$$\begin{bmatrix} (\beta_{11}+d_{11})\cdot K^{gain}_{p,int(1)} & -(\beta_{12}+d_{12})\cdot K^{gain}_{p,int(1)} & -(\beta_{13}+d_{13})\cdot K^{gain}_{p,int(1)} \\ -(\beta_{21}+d_{21})\cdot K^{gain}_{p,int(2)} & (\beta_{22}+d_{22})\cdot K^{gain}_{p,int(2)} & -(\beta_{23}+d_{23})\cdot K^{gain}_{p,int(2)} \\ -(\beta_{31}+d_{31})\cdot K^{gain}_{p,int(3)} & -(\beta_{32}+d_{32})\cdot K^{gain}_{p,int(3)} & (\beta_{33}+d_{33})\cdot K^{gain}_{p,int(3)} \end{bmatrix} \cdot \begin{bmatrix} \omega_{ref(1)}-K_{P(1)}\cdot P_{G(1)} \\ \omega_{ref(2)}-K_{P(2)}\cdot P_{G(2)} \\ \omega_{ref(3)}-K_{P(3)}\cdot P_{G(3)} \end{bmatrix} \tag{29}$$

Equation (28) includes two integrated vectors that introduce non-linearities. The first integral, e.g., $\int(\omega_j-\omega_{set})\ \forall\ j\in\{1,2,3\}$ is linearized using the equation $\int(\omega_j-\omega_{set})=\delta_j-\delta_{1in}$, where δ_1 is the angle of the positive-sequence voltage of DG *i*, while δ_{1in} is the initial angle of DG *i*, before the action of secondary control.

The second non-linear vector, e.g., $\int(\omega_{ref(j)}-K_{P(j)}\cdot P_{G(j)})$, is linearized by penalizing it with a very large number, e.g., 10^{10}. In this way, the function inside the integral is forced to zero while its influence on the droop equation is preserved. After the linearization, the non-linear system (28) is modified to the linear system (29).

Writing (29) in a more compact form, (30) is obtained:

$$[\boldsymbol{\Omega}_{ref}-\boldsymbol{\Omega}_{st}]-\boldsymbol{K_p}\cdot\boldsymbol{P_G}=\boldsymbol{ABG}\cdot[\boldsymbol{\Delta}-\boldsymbol{\Delta}_{in}]-10^{10}\cdot\boldsymbol{BD}\cdot[\boldsymbol{\Omega}_{ref}-\boldsymbol{K_p}\cdot\boldsymbol{P_G}] \tag{30}$$

where $\boldsymbol{\Omega}_{ref}=[\omega_{ref(1)}\ \ \omega_{ref(2)}\ \ \omega_{ref(3)}]^T$, $\boldsymbol{\Omega}_{st}=[\omega_{st}\ \ \omega_{st}\ \ \omega_{st}]^T$, $\boldsymbol{P_G}=[P_{G(1)}\ \ P_{G(2)}\ \ P_{G(3)}]^T$, $\boldsymbol{\Delta}=[\delta_1\ \ \delta_2\ \ \delta_3]^T$, $\boldsymbol{\Delta}_{in}=[\delta_{1in}\ \ \delta_{2in}\ \ \delta_{3in}]^T$. ω_{st} is the restored steady-state frequency, after the action of secondary control, namely 50 Hz. The matrix $\boldsymbol{K_p}$ is the square matrix of the left-hand side of (29). ***ABG*** and ***BD*** are the first and second square matrices of the right-hand side of (29). By reforming (30), equation (31) is obtained.

$$\boldsymbol{ABG}\cdot\boldsymbol{\Delta}=\boldsymbol{ABG}\cdot\boldsymbol{\Delta}_{in}+[\boldsymbol{\Omega}_{ref}-\boldsymbol{\Omega}_{st}+10^{10}\cdot\boldsymbol{BD}\cdot\boldsymbol{\Omega}_{ref}]\quad-[10^{10}\cdot\boldsymbol{BD}\cdot\boldsymbol{K_p}+\boldsymbol{K_p}]\cdot\boldsymbol{P_G} \tag{31}$$

Equation (31) relates the positive-sequence voltage angles (**Δ**) with the active powers ($\boldsymbol{P_G}$) of DGs. $\boldsymbol{P_G}$ and **Δ** are also constrained from the power flow equations since the active powers $\boldsymbol{P_G}$ affect (physically) the angles **Δ** of DGs. The objective is to find the vectors $\boldsymbol{P_G}$ and **Δ**, which satisfy, simultaneously, both the power flow equations and (31). To do that, we introduce into (31) the variables $\boldsymbol{d\Delta}$ and $\boldsymbol{dP_G}$, which denote respectively the required variations of **Δ** and $\boldsymbol{P_G}$ so that both the power flow equations and (31) are fulfilled. Introducing $\boldsymbol{d\Delta}$ and $\boldsymbol{dP_G}$ into (31), equation (32) is finally derived. Equation (32) is solved (in sub-section 5.2.3) by using sensitivities relating $\boldsymbol{d\Delta}$ and $\boldsymbol{dP_G}$, e.g., $\boldsymbol{d\Delta}=\frac{\partial\boldsymbol{\Delta}}{\partial\boldsymbol{P_G}}\boldsymbol{dP_G}$, based on the power flow equations.

$$\begin{aligned}\boldsymbol{ABG}\cdot[\boldsymbol{\Delta}+\boldsymbol{d\Delta}]=\boldsymbol{ABG}\cdot\boldsymbol{\Delta}_{in}+[\boldsymbol{\Omega}_{ref}-\boldsymbol{\Omega}_{st}+10^{10}\cdot\boldsymbol{BD}\cdot\boldsymbol{\Omega}_{ref}]\\-[10^{10}\cdot\boldsymbol{BD}\cdot\boldsymbol{K_p}+\boldsymbol{K_p}]\cdot[\boldsymbol{P_G}+\boldsymbol{dP_G}]\end{aligned} \tag{32}$$

5.2.2. Calculation of DG reactive power

Substituting the generalized equation (14) into the droop equation (2), equation system (33) is obtained for the secondary voltage control of the 6-bus MG. In (33), c_{ij}, r_{ij}, h_i, are given in Table 2, depending on the applied control strategy. Equation (33) includes one non-linear integral term, which is linearized, by penalizing the integrated function with a very large number, e.g., 10^{10}, in a similar sense as previously. Practically, $\int f(x)$ is substituted with $10^{10}\cdot f(x)$, where $f(x)$ is the integrated function. After the linearization, the non-linear system (33) is modified to the linear (34).

$$\begin{bmatrix} V_{ref(1)}-V_1-K_{Q(1)}\cdot Q_{G(1)}+K^{gain}_{q,int(1)}\cdot\int\left(h_1\cdot(V_{set(1)}-V_1)+\sum_{j=1}^{3}c_{1j}\cdot(V_j-V_1)+\sum_{j=1}^{3}r_{1j}\cdot\left(K_{Q(j)}\cdot Q_{(j)}-K_{Q(1)}\cdot Q_{(1)}\right)\right) \\ V_{ref(2)}-V_2-K_{Q(2)}\cdot Q_{G(2)}+K^{gain}_{q,int(2)}\cdot\int\left(h_2\cdot(V_{set(2)}-V_2)+\sum_{j=1}^{3}c_{2j}\cdot(V_j-V_2)+\sum_{j=1}^{3}r_{2j}\cdot\left(K_{Q(j)}\cdot Q_{(j)}-K_{Q(2)}\cdot Q_{(2)}\right)\right) \\ V_{ref(3)}-V_3-K_{Q(3)}\cdot Q_{G(3)}+K^{gain}_{q,int(3)}\cdot\int\left(h_3\cdot(V_{set(3)}-V_3)+\sum_{j=1}^{3}c_{3j}\cdot(V_j-V_3)+\sum_{j=1}^{3}r_{3j}\cdot\left(K_{Q(j)}\cdot Q_{(j)}-K_{Q(3)}\cdot Q_{(3)}\right)\right) \end{bmatrix}=\begin{bmatrix}0\\0\\0\end{bmatrix} \tag{33}$$

$$\begin{bmatrix} 1+10^{10}\cdot K^{gain}_{q,int(1)}\cdot(c_{11}+h_1) & -10^{10}\cdot K^{gain}_{q,int(1)}\cdot c_{12} & -10^{10}\cdot K^{gain}_{q,int(1)}\cdot c_{13} \\ -10^{10}\cdot K^{gain}_{q,int(2)}\cdot c_{21} & 1+10^{10}\cdot K^{gain}_{q,int(2)}\cdot(c_{22}+h_2) & -10^{10}\cdot K^{gain}_{q,int(2)}\cdot c_{23} \\ -10^{10}\cdot K^{gain}_{q,int(3)}\cdot c_{31} & -10^{10}\cdot K^{gain}_{q,int(3)}\cdot c_{32} & 1+10^{10}\cdot K^{gain}_{q,int(3)}\cdot(c_{33}+h_3) \end{bmatrix}\cdot\begin{bmatrix} V_1 \\ V_2 \\ V_3 \end{bmatrix}$$

$$= -\begin{bmatrix} K_{Q(1)}+K^{gain}_{q,int(1)}\cdot 10^{10}\cdot K_{Q(1)}\cdot r_{11} & -K^{gain}_{q,int(1)}\cdot 10^{10}\cdot K_{Q(2)}\cdot r_{12} & -K^{gain}_{q,int(1)}\cdot 10^{10}\cdot K_{Q(3)}\cdot r_{13} \\ -K^{gain}_{q,int(2)}\cdot 10^{10}\cdot K_{Q(1)}\cdot r_{21} & K_{Q(2)}+K^{gain}_{q,int(2)}\cdot 10^{10}\cdot K_{Q(2)}\cdot r_{22} & -K^{gain}_{q,int(2)}\cdot 10^{10}\cdot K_{Q(3)}\cdot r_{23} \\ -K^{gain}_{q,int(3)}\cdot 10^{10}\cdot K_{Q(1)}\cdot r_{31} & -K^{gain}_{q,int(3)}\cdot 10^{10}\cdot K_{Q(2)}\cdot r_{32} & K_{Q(3)}+K^{gain}_{q,int(3)}\cdot 10^{10}\cdot K_{Q(3)}\cdot r_{33} \end{bmatrix}\cdot\begin{bmatrix} Q_{G(1)} \\ Q_{G(2)} \\ Q_{G(3)} \end{bmatrix}+\begin{bmatrix} V_{ref(1)} \\ V_{ref(2)} \\ V_{ref(3)} \end{bmatrix}+10^{10}\cdot\begin{bmatrix} K^{gain}_{q,int(1)}\cdot h_1\cdot V_{set(1)} \\ K^{gain}_{q,int(2)}\cdot h_2\cdot V_{set(2)} \\ K^{gain}_{q,int(3)}\cdot h_3\cdot V_{set(3)} \end{bmatrix} \quad (34)$$

Writing (34) in a more compact form, (35) is obtained:

$$\boldsymbol{CH}\cdot\boldsymbol{V} = -\boldsymbol{KR}\cdot\boldsymbol{Q_G}+\boldsymbol{V_{ref}}+\boldsymbol{HV} \quad (35)$$

where $\boldsymbol{V}=[V_1 \quad V_2 \quad V_3]^T$, $\boldsymbol{Q_G}=[Q_{G(1)} \quad Q_{G(2)} \quad Q_{G(3)}]^T$, $\boldsymbol{V_{ref}}=[V_{ref(1)} \quad V_{ref(2)} \quad V_{ref(3)}]^T$. $\boldsymbol{CH}$ is the square matrix at the left-hand side of (34), $\boldsymbol{KR}$ is the square matrix at the right-hand side of (34), while $\mathbf{HV}=10^{10}\cdot\left[K^{gain}_{q,int(1)}\cdot h_1\cdot V_{set(1)} \quad K^{gain}_{q,int(2)}\cdot h_2\cdot V_{set(2)} \quad K^{gain}_{q,int(3)}\cdot h_3\cdot V_{set(3)}\right]^T$.

Finally, (36) is derived from (35), in a similar sense as (32), where $\boldsymbol{dV}$ and $\boldsymbol{dQ_G}$ are the required variation of voltage and reactive power of DGs so that both (35) and power flow equations are satisfied.

$$\boldsymbol{CH}\cdot[\boldsymbol{V}+\boldsymbol{dV}] = -\boldsymbol{KR}\cdot[\boldsymbol{Q_G}+\boldsymbol{dQ_G}]+\boldsymbol{V_{ref}}+\boldsymbol{HV} \quad (36)$$

5.2.3. Unified equation of DG powers

Equation systems (32) and (36) are unified in a single system, as shown in (37).

$$\begin{bmatrix} \boldsymbol{ABG} & 0 \\ 0 & \boldsymbol{CH} \end{bmatrix}\cdot\begin{bmatrix} \boldsymbol{d\Delta} \\ \boldsymbol{dV} \end{bmatrix}=\begin{bmatrix} \boldsymbol{ABG} & 0 \\ 0 & \boldsymbol{CH} \end{bmatrix}\cdot\begin{bmatrix} \boldsymbol{\Delta_{in}}-\boldsymbol{\Delta} \\ -\boldsymbol{V} \end{bmatrix}-\begin{bmatrix} \boldsymbol{M_a} & 0 \\ 0 & \boldsymbol{KR} \end{bmatrix}\cdot\begin{bmatrix} \boldsymbol{dP_G} \\ \boldsymbol{dQ_G} \end{bmatrix}+\begin{bmatrix} \boldsymbol{M_b} \\ \boldsymbol{HV}+\boldsymbol{V_{ref}}-\boldsymbol{KR}\cdot\boldsymbol{Q_G} \end{bmatrix} \quad (37)$$

where $\boldsymbol{M_a}=10^{10}\cdot\boldsymbol{BD}\cdot\boldsymbol{K_p}+\boldsymbol{K_p}$ and $\boldsymbol{M_b}=\boldsymbol{\Omega_{ref}}-\boldsymbol{\Omega_{st}}+10^{10}\cdot\boldsymbol{BD}\cdot\boldsymbol{\Omega_{ref}}-\left[10^{10}\cdot\boldsymbol{BD}\cdot\boldsymbol{K_p}+\boldsymbol{K_p}\right]\cdot\boldsymbol{P_G}$

Equation system (37) can be written in a more compact form as follows:

$$\boldsymbol{A_f}\cdot\begin{bmatrix} \boldsymbol{d\Delta} \\ \boldsymbol{dV} \end{bmatrix}=\boldsymbol{A_f}\cdot\begin{bmatrix} \boldsymbol{\Delta_{in}}-\boldsymbol{\Delta} \\ -\boldsymbol{V} \end{bmatrix}-\boldsymbol{B_f}\cdot\begin{bmatrix} \boldsymbol{dP_G} \\ \boldsymbol{dQ_G} \end{bmatrix}+\boldsymbol{C_f} \quad (38)$$

where $\boldsymbol{A_f}=\begin{bmatrix} \boldsymbol{ABG} & 0 \\ 0 & \boldsymbol{CH} \end{bmatrix}$, $\boldsymbol{B_f}=\begin{bmatrix} \boldsymbol{M_a} & 0 \\ 0 & \boldsymbol{KR} \end{bmatrix}$, $\boldsymbol{C_f}=\begin{bmatrix} \boldsymbol{M_b} \\ \boldsymbol{HV}+\boldsymbol{V_{ref}}-\boldsymbol{KR}\cdot\boldsymbol{Q_G} \end{bmatrix}$.

Considering the sensitivity matrix $\boldsymbol{Sens}=\begin{bmatrix} \frac{\partial\boldsymbol{\Delta}}{\partial\boldsymbol{P_G}} & \frac{\partial\boldsymbol{\Delta}}{\partial\boldsymbol{Q_G}} \\ \frac{\partial\boldsymbol{V}}{\partial\boldsymbol{P_G}} & \frac{\partial\boldsymbol{V}}{\partial\boldsymbol{Q_G}} \end{bmatrix}$, equation (38) is written as follows in (39).

$$\boldsymbol{A_f}\cdot\boldsymbol{Sens}\cdot\begin{bmatrix} \boldsymbol{dP_G} \\ \boldsymbol{dQ_G} \end{bmatrix}=\boldsymbol{A_f}\cdot\begin{bmatrix} \boldsymbol{\Delta_{in}}-\boldsymbol{\Delta} \\ -\boldsymbol{V} \end{bmatrix}-\boldsymbol{B_f}\cdot\begin{bmatrix} \boldsymbol{dP_G} \\ \boldsymbol{dQ_G} \end{bmatrix}+\boldsymbol{C_f} \quad (39)$$

It is noted that the elements of ***Sens*** matrix are calculated in a *perturb and observe* way, by observing the angle ($\boldsymbol{d\Delta}$) and voltage ($\boldsymbol{dV}$) variations, after the injection of small perturbation powers ($\boldsymbol{dP_G}$, $\boldsymbol{dQ_G}$). Due to space limitation, an extensive analysis about the elements of ***Sens*** is not possible here. More details are provided in [30, Section 3.2].

From (39), equation (40) is finally derived, which calculates the required variation of DG powers so that the steady state of secondary controllers and power flow constraints are satisfied. Note that in (40), the vectors $\boldsymbol{\Delta}, \boldsymbol{V}$ and matrices $\boldsymbol{Sens}, \boldsymbol{C_f}$ are updated in each power flow iteration, based on the results of the last power flow iteration, while matrices $\boldsymbol{A_f}$, $\boldsymbol{B_f}$ are constant.

$$\begin{bmatrix} \boldsymbol{dP_G} \\ \boldsymbol{dQ_G} \end{bmatrix}=\left(\boldsymbol{A_f}\cdot\boldsymbol{Sens}+\boldsymbol{B_f}\right)^{-1}\cdot\left(\boldsymbol{A_f}\cdot\begin{bmatrix} \boldsymbol{\Delta_{in}}-\boldsymbol{\Delta} \\ -\boldsymbol{V} \end{bmatrix}+\boldsymbol{C_f}\right) \quad (40)$$

Table 4
Steady State Results of Decentralized Secondary Control of 6-Bus MG.

	Proposed	Simulink
Frequency (Hz)	50	50
Voltage DG 1 (V)	230	230
Voltage DG 1 (V)	230	230
Voltage DG 1 (V)	230	230
Voltage angle DG 1 (rads)	0.6248	–
Voltage angle DG 2 (rads)	0.6286	–
Voltage angle DG 3 (rads)	0.5896	–
Active/Reactive power DG 1 (kW)	51.1 + 5.7j	51.1 + 5.7j
Active/Reactive power DG 2 (kW)	49.7–17.4j	49.7–17.4j
Active/Reactive power DG 3 (kW)	59.4 + 62.6j	59.4 + 62.6j

5.3. Flowchart of the Proposed Approach

A flowchart of the proposed modelling approach is given in Fig. 4, consisting of one initialization step and two repetitive steps.

6. Validation of the Proposed Approach

The results of the proposed method are validated here against the dynamic results of Simulink, using the 6-Bus MG of Fig. 1.

6.1. Description of the Network

The parameters of the examined 6-Bus MG are shown in Table 5. It is an unbalanced MG with constant impedance loads. All DGs have the same capacity and primary droop parameters[1]. In the next sub-sections, several scenarios are investigated, for all communication strategies, to highlight the accuracy and benefits of proposed method.

6.2. Results of decentralized strategy

The graph of decentralized control of the examined 6-Bus MG is shown in Fig. 2a. Two scenarios are investigated:

- *Scenario 1*: The integral gains of the PI controllers in (3) and (4) are set $K^{gain}_{p,int(i)}=K^{gain}_{q,int(i)}=4 \quad \forall i\in\{1,2,3\}$.
- *Scenario 2*: The integral gains of the PI controllers in (3) and (4) are set $K^{gain}_{p,int(i)}=K^{gain}_{q,int(i)}=0.5 \quad \forall i\in\{1,2,3\}$.

[1] The same DG parameters were used for the sake of simplicity. A more complex case study is provided in the supplementary file.

Table 5
Parameters of 6-Bus AC Microgrid.

Resistance of the lines	0.5 Ohm/km
Self-Reactance of the lines	0.6 mH/km
Mutual-Reactance of the lines	0.1 mH/km
Line lengths	0.1 km
Unbalanced Load 1 (phase A), (phase B), (phase C)	(2 Ohm // 0.02H), (3 Ohm // 0.03H), (4 Ohm // 0.04H),
Unbalanced Load 2 (phase A), (phase B), (phase C)	(1 Ohm // 0.01*H*), (2 Ohm // 0.02H), (2 Ohm // 0.02H),
Droop gain $K_{P(i)}$ $(i = 1, 2, 3)$	$2\pi{\cdot}2{\cdot}10^{-6}$ (rad·s^{-1}/W)
Droop gain $K_{Q(i)}$ $(i = 1, 2, 3)$	$2{\cdot}10^{-4}$ (V/VAR)
Reference $V_{ref(i)}(i = 1, 2, 3)$	230 V
Reference $\omega_{ref(i)}$ $(i = 1, 2, 3)$	$2\pi{\cdot}50$ rads/s
DG Capacity	100 kVA
Grounding resistances	25 Ohm

It is noted that the proportional gains do not affect the steady state results, because after the restoration, the proportional term is nullified. In both scenarios, the voltage and frequency are restored to 230 V and 50 Hz, respectively. The powers of DGs after the action of secondary controller, are depicted in Table 6, for the two scenarios, using the proposed method (with black) and Simulink (with red).

As shown, in both scenarios, the results of the proposed method are identical with those of Simulink, confirming its accuracy. Moreover, the powers of DGs differ due to the different dynamic histories of integrated functions $(\omega_{set(i)} - \omega_i)$. Specifically, although $\omega_{set(i)}$ is the same $\forall i \in \{1, 2, 3\}$, ω_i is dynamically varied, unequally for the three DGs, during the response of secondary controller, yielding different integrals.

6.3. Results of Centralized Strategy

The communication graph of centralized control is shown in Fig. 2b. It is assumed that the MGCC measures the frequency and voltage at the connection point of DG 1. Three scenarios are investigated:

- *Scenario 1*: There are no communication failures . The integral gain of MGCC is $K^{gain}_{p,int} = K^{gain}_{q,int} = 4$.
- *Scenario 2*: The communication link between the MGCC and DG 2 is out of service. It is noted that a communication link can be failed due to several reasons such as a physical damage or a protective disconnection of a corrupted link after a cyberattack [31, Section 4]. The integral gain of MGCC is $K^{gain}_{p,int} = K^{gain}_{q,int} = 4$.
- *Scenario 3*: The communication link between the MGCC and DG 2 is out of service. The integral gain of MGCC is $K^{gain}_{p,int} = K^{gain}_{q,int} = 0.5$.

It is noted that due to the disconnection of the link in scenarios 2 and 3, the matrices $\boldsymbol{g}, \boldsymbol{\alpha}, \boldsymbol{h}, \boldsymbol{c}$ of Tables 1 and 2 should be suitably reformed to model the link outage. More specifically, the elements of the 2nd row of matrices $\boldsymbol{\alpha}$, $\boldsymbol{c}$ and the 2nd element of $\boldsymbol{g}, \boldsymbol{h}$ should be nullified.

As shown in Table 7, the results of the proposed approach are identical with those of Simulink. Moreover, after the communication outage, the active and the reactive power of DGs have been completely changed and the equal power sharing has been lost.

Table 6
Decentralized Control: Powers of DGs* (in kW, kVar).

	DG 1	DG 2	DG 3
Scenario 1	51.1 + 5.7j 51.1 + 5.7j	49.7 – 17.4j 49.7 – 17.4j	59.4+ 62.6j 59.4 + 62.6j
Scenario 2	53.3 – 0.49j 53.3 – 0.49j	53.2 – 26.9j 53.2 – 26.9j	55.0 + 78.9j 55.0 + 78.9j

*The positive sign of powers denotes power production. Red numbers denote the results of Simulink.

Table 7
Centralized Control: Powers of DGs (in kW, kVar).

	DG 1	DG 2	DG 3
Scenario 1	52.4 + 12.5j 52.4 + 12.5j	52.4 + 10.7j 52.4 + 10.7j	52.4 + 26.8j 52.4 + 26.8j
Scenario 2	78.1 + 2.2j 78.1 + 2.2j	0 + 31.2j 0 + 31.2j	78.1 + 16.3j 78.1 + 16.3j
Scenario 3	78.1 + 2.2j 78.1 + 2.2j	0 + 31.2j 0 + 31.2j	78.1 + 16.3j 78.1 + 16.3j

6.4. Results of Distributed Averaging Strategy

The communication graph of distributed averaging control is shown in Fig. 2c. Two scenarios are investigated:

- *Scenario 1*: There are no communication failures . The integral gains of the three DGs are $K^{gain}_{p,int(i)} = K^{gain}_{q,int(i)} = 4 \quad \forall i \in \{1, 2, 3\}$.
- *Scenario 2*: The communication of DG 1 is failed, thus, the DG links 1–2 and 1–3 are out of service. The integral gains of DGs are $K^{gain}_{p,int(i)} = K^{gain}_{q,int(i)} = 4 \quad \forall i \in \{1, 2, 3\}$.

To model the communication failures of links 1–2 and 1–3, the matrices $\boldsymbol{a}, \boldsymbol{c}, \boldsymbol{r}$ of Tables 1 and 2 are modified, as follows: $\boldsymbol{\alpha} = \boldsymbol{c} = -\boldsymbol{r} = -\begin{bmatrix} 0 & 0 & 0 \\ 0 & 1/2 & 1/2 \\ 0 & 1/2 & 1/2 \end{bmatrix}$. Again, the results of the proposed approach shown in Table 8 coincide completely with Simulink. Moreover, the links' outage in scenario 2 deteriorates the power sharing of DGs.

6.5. Results of Consensus Strategy

The communication graph of consensus control is shown in Fig. 2d. Due to space limitation, only the two cases of Simpson's method [24] are investigated. Specifically, case 1 performs equal DG reactive power sharing, while case 2 voltage regulation. The frequency controller is the same for both cases.

Five scenarios are investigated:

- *Scenario 1*: The voltage controller operates in voltage regulation mode (case 2 of [24]). There are no communication failures. The integral gains of DGs are $K^{gain}_{p,int(i)} = K^{gain}_{q,int(i)} = 4 \quad \forall i \in \{1, 2, 3\}$. All DGs are assumed pinned, namely $\boldsymbol{g} = [1 \quad 1 \quad 1]$.
- *Scenario 2*: The voltage controller operates in reactive power sharing mode (case 1 of [24]). There are no communication failures . The integral gains are $K^{gain}_{p,int(i)} = K^{gain}_{q,int(i)} = 4 \quad \forall i \in \{1, 2, 3\}$. All DGs are assumed pinned, namely $\boldsymbol{g} = [1 \quad 1 \quad 1]$.
- *Scenario 3*: The voltage controller operates in reactive power sharing mode (case 1 of [24]). Communication link 1–2 is out of service, while $K^{gain}_{p,int(i)} = K^{gain}_{q,int(i)} = 4 \quad \forall i \in \{1, 2, 3\}$. Due to the communication failure, the matrices $\boldsymbol{\beta}, \boldsymbol{r}$ of Tables 1, 2 need to be modified accordingly. All DGs are assumed pinned.
- *Scenario 4*: The voltage controller operates in reactive power sharing mode (case 1 of [24]). Communication link 1–2 is out of service,

Table 8
Distributed Averaging: Powers of DGs (in kW, kVar).

	DG 1	DG 2	DG 3
Scenario 1	52.8 + 16.8j 52.8 + 16.8j	52.8 + 16.8j 52.8 + 16.8j	52.8 + 16.8j 52.8 + 16.8j
Scenario 2	50.5 – 2.3j 50.5 – 2.3j	54.1 + 26.4j 54.1 + 26.4j	54.1 + 26.4j 54.1 + 26.4j

Table 9
Consensus Control: Powers of DGs (in kW, kVar).

	DG 1	DG 2	DG 3
Scenario 1	54.0 -2.3j 54.0 -2.3j	54.0 – 29.0j 54.0 – 29.0j	54.0 + 82.8j 54.0 + 82.8j
Scenario 2	51.3 + 16.3j 51.3 + 16.3j	51.3 + 16.3j 51.3 + 16.3j	51.3 + 16.3j 51.3 + 16.3j
Scenario 3	51.5 + 11.8j 51.5 + 11.8j	51.2 + 18.6j 51.2 + 18.6j	51.2 + 18.6j 51.2 + 18.6j
Scenario 4	167 – 44.5j 167 – 44.5j	0 + 48.8j 0 + 48.8j	0 + 48.8j 0 + 48.8j
Scenario 5	0 + 40.6j 0 + 40.6j	78.4 + 4.6j 78.4 + 4.6j	78.4 + 4.6j 78.4 + 4.6j

while $K^{gain}_{p,int(i)} = K^{gain}_{q,int(i)} = 4 \quad \forall i \in \{1,2,3\}$. Only DG 1 is assumed pinned ($\boldsymbol{g} = [1 \quad 0 \quad 0]$).

- *Scenario 5*: The voltage controller operates in reactive power sharing mode (case 1 of [24]). Communication link 1–2 is out of service, while $K^{gain}_{p,int(i)} = K^{gain}_{q,int(i)} = 4 \quad \forall i \in \{1,2,3\}$. Only DG 2 is assumed pinned ($\boldsymbol{g} = [0 \quad 1 \quad 0]$).

The results are shown in Table 9, where the accuracy of the proposed approach is again confirmed against Simulink. Several observations can be made from Table 9: a) the control mode of voltage controller can significantly affect the steady state of secondary control, as shown from the differences of scenario 1 and 2, b) a communication failure deteriorates the power sharing between the DGs in consensus schemes, as follows from the differences in scenarios 2 and 3, c) the pinning of DGs can affect their power production, in case of communication failures, as shown from the differences in scenarios 3, 4 and 5. Moreover, in scenario 4 the DG 1 may exceeds its maximum capacity, which can affect the stability of the MG.

7. Simulations in the IEEE 8500-Node Network

To test the scalability of the proposed method, simulations are executed in a modified islanded version of the IEEE 8500-node network [37], consisting of 7 DGs, as shown in Fig. 5.

7.1. Description of the Network

The data of the MG are referred in Table 10. The DGs operate in consensus control, using the method of Bidram [22]. The communication graph between the DGs is shown in Fig. 6.

7.2. Investigated Scenarios

Four scenarios are investigated:

- *Scenario 1*: There are no communication failures. DG 1, 3, 7 are pinned. The integral gains of secondary controllers are $K^{gain}_{p,int(i)} = K^{gain}_{q,int(i)} = 2 \quad \forall i \in \{1,2,3,4,5,6,7\}$. The corresponding matrices $\boldsymbol{\alpha}, \boldsymbol{d}, \boldsymbol{h}, \boldsymbol{c}, \boldsymbol{g}$ of Tables 1, 2 for the communication graph of Fig. 6 are as follows:

$$\boldsymbol{\alpha} = \boldsymbol{d} = \boldsymbol{c} = \begin{bmatrix} 2 & 1 & 0 & 1 & 0 & 0 & 0 \\ 1 & 2 & 1 & 0 & 0 & 0 & 0 \\ 0 & 1 & 1 & 0 & 0 & 0 & 0 \\ 1 & 0 & 0 & 2 & 1 & 0 & 0 \\ 0 & 0 & 0 & 1 & 3 & 1 & 1 \\ 0 & 0 & 0 & 0 & 1 & 1 & 0 \\ 0 & 0 & 0 & 0 & 1 & 0 & 1 \end{bmatrix}$$

$$\boldsymbol{h} = \boldsymbol{g} = [1 \quad 0 \quad 1 \quad 0 \quad 0 \quad 0 \quad 1]$$

- *Scenario 2*: The link connecting DGs 4 and 5 is out of service. DG 1, 3, 7 are pinned. The integral gains of DG controllers are $K^{gain}_{p,int(i)} = K^{gain}_{q,int(i)} = 2 \quad \forall i \in \{1,2,3,4,5,6,7\}$. Due to the communication failure, the 4th and 5th rows of the matrices $\boldsymbol{\alpha}, \boldsymbol{d}, \boldsymbol{c}$ should be modified accordingly:

$$\boldsymbol{\alpha} = \boldsymbol{d} = \boldsymbol{c} = \begin{bmatrix} 2 & 1 & 0 & 1 & 0 & 0 & 0 \\ 1 & 2 & 1 & 0 & 0 & 0 & 0 \\ 0 & 1 & 1 & 0 & 0 & 0 & 0 \\ 1 & 0 & 0 & 1 & 0 & 0 & 0 \\ 0 & 0 & 0 & 0 & 2 & 1 & 1 \\ 0 & 0 & 0 & 0 & 1 & 1 & 0 \\ 0 & 0 & 0 & 0 & 1 & 0 & 1 \end{bmatrix}$$

- *Scenario 3*: The link connecting DGs 4 and 5 is out of service. The DG 1, 3, 7 are pinned. The integral gains of the DG controllers are $K^{gain}_{p,int(i)} = K^{gain}_{q,int(i)} = 10 \quad \forall i \in \{1,2,3,4,5,6,7\}$.
- *Scenario 4*: The link connecting DGs 4 and 5 is out of service. The DG 1, 3 are pinned. The integral gains of the DG controllers are $K^{gain}_{p,int(i)} = K^{gain}_{q,int(i)} = 10 \quad \forall i \in \{1,2,3,4,5,6,7\}$. Since in this scenario DG 7 is unpinned, the matrices $\boldsymbol{h} = \boldsymbol{g} = [1 \quad 0 \quad 1 \quad 0 \quad 0 \quad 0 \quad 0]$.

The power of DGs for the four examined scenarios are depicted in Table 11, from which the following deductions are derived:

- A comparison between scenarios 1 and 2 indicate that a communication failure can affect, seriously, the power sharing between the DGs.
- A rise in the integral gain of secondary controller influences the steady-state condition of the MG, as shown from the differences between scenarios 2 and 3.

Table 10
Data of the 8500-Node Network.

Line Lengths	Given in [37]
Resistance of the lines	Given in [37]
Reactance of the lines	Given in [37]
Active power load of each phase	Given in [37]
Total active power load	10.7 MW [37]
Power factor of each phase	0.97 inductive
Phase-to-neutral nominal voltage	7.2 kV
Droop gain $K_{P(i)}$ (i = 1,2,3,4,5,6,7)	$2\pi{\cdot}10^{-6}$ (rad·s^{-1}/W)
Droop gain $K_{Q(i)}$ (i = 1,2,3,4,5,6,7)	$1{\cdot}10^{-4}$ (V/VAR)
Reference $V_{ref(i)}$ (i = 1,2,3,4,5,6,7)	7.2 kV
Reference $\omega_{ref(i)}$ (i = 1,2,3,4,5,6,7)	$2\pi{\cdot}50$ rads/s
Grounding resistances	25 Ohm

Table 11
Power of DGs (MW, MVAR)* Using the Proposed Approach.

	Scenario 1	Scenario 2	Scenario 3	Scenario 4
DG 1	1.61 + 1.91j	1.87 + 2.23j	1.76 + 2.10j	3.37 + 3.75j
DG 2	1.61 + 0.92j	1.87 + 0.93j	1.76 + 0.92j	3.37 + 1.28j
DG 3	1.61 – 1.78j	1.87 – 2.31j	1.76 – 2.09j	3.37 – 4.85j
DG 4	1.61 – 0.02j	1.87 – 0.14j	1.76 – 0.09j	3.37 + 1.31j
DG 5	1.61 + 3.39j	1.31 + 2.83j	1.44 + 3.06j	0.00 – 1.56j
DG 6	1.61 – 1.19j	1.31 – 0.64j	1.44 – 0.87j	0.00 + 2.24j
DG 7	1.61 – 0.23j	1.31 + 0.14j	1.44 – 0.01j	0.00 + 2.05j

*The positive sign of powers denotes power production.

Table 12
Power of DGs (MW, MVAR) Using the Conventional Power Flow of [2–5].

	Scenario 1	Scenario 2	Scenario 3	Scenario 4
DG 1	1.61 + 1.91j	1.61 + 1.91j	1.61 + 1.91j	1.61 + 1.91j
DG 2	1.61 + 0.92j	1.61 + 0.92j	1.61 + 0.92j	1.61 + 0.92j
DG 3	1.61 − 1.78j	1.61 − 1.78j	1.61 − 1.78j	1.61 − 1.78j
DG 4	1.61 − 0.02j	1.61 − 0.02j	1.61 − 0.02j	1.61 − 0.02j
DG 5	1.61 + 3.39j	1.61 + 3.39j	1.61 + 3.39j	1.61 + 3.39j
DG 6	1.61 − 1.19j	1.61 − 1.19j	1.61 − 1.19j	1.61 − 1.19j
DG 7	1.61 − 0.23j	1.61 − 0.23j	1.61 − 0.23j	1.61 − 0.23j

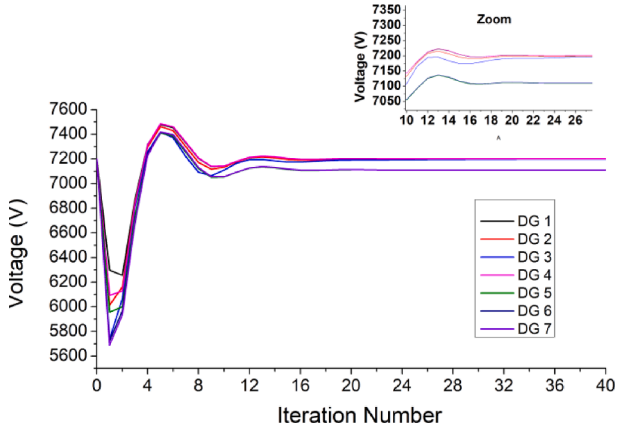

Fig. 7. Convergence of the positive-sequence voltages of DGs for scenario 4 of IEEE 8500-node network.

- The pinning of DGs can lead to significant deviations in the active power sharing between the DGs, after a communication failure, as highlighted from the different results of scenarios 3 and 4.

It is clearly highlighted that a communication failure can affect, significantly, the secondary control of an islanded MG. The steady-state condition of secondary control depends on several factors such as the control mode (e.g centralized, decentralized, distributed averaging, consensus etc.), the pinning of DGs, the integral gains of PI controllers, the position of failed communication link etc. The proposed approach considers all these factors, and thus, it can constitute an accurate tool for modelling the steady-state of secondary control in islanded MGs.

In contrast, as shown in Table 12, conventional power flow methods [2–5] present the same results in all scenarios, since they consider (1)-(2), assuming always that $u_{p(i)} = u_{q(i)} = 0 \quad \forall i \in \{1,2,3,4,5,6,7\}$. As a result, they can model precisely only scenario 1, where the power sharing depends only on the droop parameters ($K_{P(i)}$). On the opposite, in case of communication failures, such as scenarios 2, 3, 4, the methods of [2–5] present considerable inaccuracies. Finally, the methods of [6–13] are not applicable here, due to their inability to handle unbalanced networks.

Regarding the computation time, the proposed approach converges in around 40 iterations with an accuracy of 10^{-4} pu, when applied in the IEEE 8500-Node network. Since every iteration requires around 0.2 sec, the total computation time of the method is around 8 s. Considering the large size and the precise mathematical representation (3-phase) of the MG, this time is reasonable.

Finally, the convergence speed of the proposed approach, for scenario 4, is illustrated in Fig. 7. As shown, the convergence is adequate. Another important thing to note is that DGs 5, 6 and 7 do not restore their voltage to 7200 V, because in scenario 4, these DGs have lost the access to the reference voltage (7200 V) since they are unpinned and the communication link 4–5 is out of service.

8. Conclusion and Future Research

This paper proposes a three-phase steady-state modelling approach for simulating the secondary control of unbalanced islanded microgrids. It is generic and can be applied in all control schemes, e.g., decentralized, centralized, distributed averaging, consensus. It presents low computation time with high accuracy since it considers all the crucial factors that can affect the steady-state condition of secondary control such as communication links, proportional and integral gains of secondary controllers, pinning of DGs. Although the paper addresses an important gap in the modelling of islanded microgrids, there are still open issues that cannot be fully addressed in a single publication. For instance, the proposed method is applicable only when the input of secondary PI controllers is a linear function such as decentralized, centralized, distributed averaging, linear consensus etc. In case of non-linear controllers, such as [29, Eqs. (28), (35)], new modelling methods need to be invented and left for future research.

CRediT authorship contribution statement

Evangelos E. Pompodakis: Conceptualization, Methodology, Software, Validation, Formal analysis, Investigation, Resources, Writing – original draft, Writing – review & editing. **Gibran D.A. Tinajero:** Writing – review & editing. **Emmanuel S. Karapidakis:** Writing – review & editing, Supervision, Funding acquisition.

Declaration of Competing Interest

The authors declare that they have no known competing financial interests or personal relationships that could have appeared to influence the work reported in this paper.

Data availability

No data was used for the research described in the article.

Appendix A

Fig. 8a shows the voltage vectors of DGs, during the primary control of 6-bus network of Fig. 1. The reference frame and voltage vectors are all (synchronously) rotated with 49.8974 Hz (see Table 3). The voltage angles of DGs are $\delta_{1in}, \delta_{2in}, \delta_{3in}$ with respect to the reference frame.

After the activation of secondary control, the reference frame is rotated with 50 Hz ($\omega_{set(i)} = 50Hz \; \forall \; i \in \{1,2,3\}$) and voltage vectors gradually increase their rotational speed through the PI controller to reach 50 Hz. During the period between the activation and stabilization of secondary controller, the rotational speed of voltage vectors differs from that of reference frame (namely $\omega_j \neq 50 \; Hz \quad \forall i \in \{1,2,3\}$), and thus, voltage angles are shifted from their initial values e.g., $\delta_j \neq \delta_{jin} \; \forall \; i \in \{1,2,3\}$, according to (41).

$$\int (\omega_{set(j)} - \omega_j) = \delta_{jin} - \delta_j \qquad \forall j = \{1,2,3\} \tag{41}$$

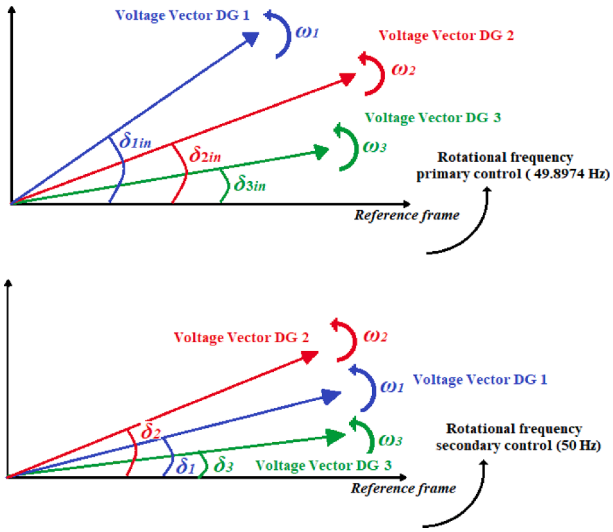

Fig. 8. From top to bottom: Reference frame and voltage vectors of DGs in a) primary, b) secondary control.

References

[1] Chopra S, et al. Power-flow-based energy management of hierarchically controlled islanded AC microgrids. Int J Electr Power Energy Syst 2022;141:108140.
[2] Pompodakis EE, Kryonidis GC, Alexiadis MC. A comprehensive load flow approach for grid-connected and islanded AC microgrids. Trans Power Syst 2020;35(2): 1143–55.
[3] Pompodakis EE, et al. A Generic Power Flow Algorithm for Unbalanced Islanded Hybrid AC/DC Microgrids. IEEE Trans Power Syst 2021; 36(2).
[4] Abdelaziz MMA, Farag HE, El-Saadany EF, Mohamed YAI. A novel and generalized three-phase power flow algorithm for islanded microgrids using a Newton trust region method. IEEE Trans Power Syst Feb. 2013;28(1):190–201.
[5] Allam MA, Hamad AA, Kazerani M. A generic modeling and power-flow analysis approach for isochronous and droop-controlled microgrids. IEEE Trans Power Syst Sep. 2018;33(5):5657–70.
[6] Mumtaz F, Syed MH, Hosani MA, Zeineldin HH. A novel approach to solve power flow for islanded microgrids using modified Newton Raphson with droop control of DG. IEEE Trans Sustain Energy Apr. 2016;7(2):493–503.
[7] Rese L, Simões Costa A, Silva AS. A modified load flow algorithm for microgrids operating in islanded mode. Proc. IEEE PES Conf. Innovative Smart Grid Technol., pp. 1-7, 2013.
[8] Mumtaz F, et al. A simple and accurate approach to solve the power flow for balanced islanded microgrids. Proc. 15th Int. Conf. Environ. Electr. Eng., pp. 1852-1856, 2015.
[9] Moradi MH, et al. Power flow analysis in islanded Micro-Grids via modeling different operational modes of DGs: A review and a new approach. Renew Sustain Energy Rev 2017:248–62.
[10] Kryonidis GC, Kontis EO, Chrysochos AI, Oureilidis KO, Demoulias CS, Papagiannis GK. Power flow of islanded AC microgrids: Revisited. IEEE Trans Smart Grid Jul. 2018;9(4):3903–5.
[11] Diaz G, Gómez-Aleixandre J, Coto J. Direct backward/forward sweep algorithm for solving load power flows in AC droop-regulated microgrids. IEEE Trans Smart Grid Sep. 2016;7(5):2208–17.
[12] Nassar M, Salama M. A novel branch-based power flow algorithm for islanded AC microgrids. Elect Power Syst Res 2017:51–62.
[13] Hameed F, Hosani MA, Zeineldin HH. A modified backward/forward sweep load flow method for islanded radial microgrids. IEEE Trans Smart Grid Jan. 2019;10 (1):910–8.
[14] Marti P, Velasco M, Martn EX, de Vicua LG, Miret J, Castilla M. Performance evaluation of secondary control policies with respect to digital communications properties in inverter-based islanded microgrids. IEEE Trans Smart Grid May 2018; 9(3):2192–202.
[15] Velasco M, Martí P, Camacho A, Miret J, Castilla M. Synchronization of local integral controllers for frequency restoration in islanded microgrids. Proc. 42nd Annu. Conf. IEEE Ind. Electron. Soc., pp. 3906-3911, 2016.
[16] Castilla M, et al. "Impact of Clock Drifts on Communication-Free Secondary Control Schemes for Inverter-Based Islanded Microgrids. IEEE Trans Ind Electronics June 2018;65(6).
[17] Khayat Y, et al. Decentralized optimal frequency control in autonomous microgrids. IEEE Trans Power Syst May 2019;34(3):2345–53.
[18] Tinajero GDA, et al. Power flow modeling of islanded AC microgrids with hierarchical control. Int J Electr Power Energy Syst 2019:28–36.
[19] Shafiee Q, Guerrero JM, Vasquez JC. Distributed secondary control for islanded microgrids—A novel approach. IEEE Trans Power Electron Feb. 2014;29(2): 1018–31.
[20] Wei B, Gui Y, Trujillo S, Guerrero JM, Vasquez JC. Distributed average integral secondary control for modular UPS systems-based microgrids. IEEE Trans Power Electron Jul. 2019;34(7):6922–36.
[21] Nguyen TL, Nguyen HT, Wang Y, Mohammed OA, Anagnostou E. Distributed Secondary Control in Microgrids Using Synchronous Condenser for Voltage and Frequency Support. Energies 2022;15:2968. https://doi.org/10.3390/en15082968.
[22] Bidram A, et al. Secondary control of microgrids based on distributed cooperative control of multi-agent systems. IET Gener, Transmission Distrib 2013; 7(8): pp. 822-831.
[23] Manaffam S, et al. Intelligent Pinning Based Cooperative Secondary Control of Distributed Generators for Microgrid in Islanding Operation Mode. IEEE Trans Power Systems 2018;33(2):pp.
[24] Simpson-Porco JW, et al. Secondary frequency and voltage control of islanded microgrids via distributed averaging. IEEE Trans Ind Electron 2015; 62(11): 7025–7038.
[25] Simpson-Porco John W, et al. Stability, Power Sharing, & Distributed Secondary Control in Droop-Controlled Microgrids. Conference: IEEE International Conference on Smart Grid Communications, 2013.
[26] Ren L, et al. Generalized Microgrid Power Flow. IEEE Trans Smart Grid 2018; 9(4): 3911-3913.
[27] Feng F, et al. Enhanced Microgrid Power Flow Incorporating Hierarchical Control. IEEE Trans Power Syst 2020; 35(3): 2463-2466.
[28] Gap F, et al. Primary and secondary control in DC microgrids: a review. J Mod Power Syst Clean Energy 2019; 7: 227–242.
[29] Dehkordi NM, et al. Distributed robust finite-time secondary voltage and frequency control of islanded microgrids. IEEE Trans Power Syst 2017; 32(5): 3648-3659.
[30] Pompodakis, Evangelos et al. A Three-Phase Sensitivity-Based Approach for Smooth Line-Switching in Islanded Microgrids. Int J Electr Power Energy Syst 2023; 144: 108515.
[31] Zhou Q, et al. A cyber-attack resilient distributed control strategy in islanded microgrids. IEEE Trans Smart Grid 2020; 11(5): 3690-3701.
[32] Hui H, et al. Coordination control of distributed generators and load resources for frequency restoration in isolated urban microgrids. Appl Energy 2022; 327: 120116.
[33] Ren L, et al. Enabling resilient distributed power sharing in networked microgrids through software defined networking. Appl Energy 2018; 210: 1251-1265.
[34] Hongfei Xiao et al. Parameterized and centralized secondary voltage control for autonomous microgrids. Int J Electr Power Energy Syst 2022; 135: 107531.
[35] Zhao G, et al. Distributed Dynamic Event-Triggered Secondary Control for Islanded Microgrids with Disturbances and Communication Delays: A Hybrid Systems Approach. IEEE Transactions on Industrial Informatics, Early Access 2022.
[36] Li Z, Cheng Z, Si J, Li S. Distributed Event-Triggered Hierarchical Control to Improve Economic Operation of Hybrid AC/DC Microgrids. IEEE Trans Power Syst Sept. 2022;37(5):3653–68.
[37] IEEE PES. (2021, October.) Distribution test feeders, "8500-Node Test Feeder". [Online]. Available: http://www.ewh.ieee.org/soc/pes/dsacom/testfeeders/index.html.